Morphometric and Mechanical Analyses of Calcifications and Fibrous Plaque Tissue in Carotid Arteries for Plaque Rupture Risk Assessment

Frank J. H. Gijsen, Bas Vis, Hilary E. Barrett, Amir A. Zadpoor, Hence J. Verhagen, Daniel Bos, Anton F. W. van der Steen, Ali C. Akyildiz*

***Abstract*— *Objective:* Atherosclerotic plaque rupture in carotid arteries is a major source of cerebrovascular events. Calcifications are highly prevalent in carotid plaques, but their role in plaque rupture remains poorly understood. This work studied the morphometric features of calcifications in carotid plaques and their effect on the stress distribution in the fibrous plaque tissue at the calcification interface, as a potential source of plaque rupture and clinical events. *Methods:* A comprehensive morphometric analysis of 65 histology cross-sections from 16 carotid plaques was performed to identify the morphology (size and shape) and location of plaque calcifications, and the fibrous-tissue fiber organization around them. Calcification-specific finite element models were constructed to examine the fibrous plaque tissue stresses at the calcification interface. Statistical correlation analysis was performed to elucidate the impact of calcification morphology and fibrous tissue organization on interface stresses. *Results:* Hundred-seventy-one calcifications were identified on the histology cross-sections, which showed great variation in morphology. Four distinct patterns of fiber organization in the plaque tissue were observed around the calcification. They were termed as attached, pushed-aside, encircling and random patterns. The stress analyses showed that calcifications are correlated with high interface stresses, which might be comparable to or even above the plaque strength. The stress levels depended on the calcification morphology and fiber organization. Thicker calcification with a circumferential slender shape, located close to the lumen were correlated most prominently to high interface stresses. *Conclusion*: Depending on its morphology and the fiber organization around it, a calcification in an atherosclerotic plaque can act as a stress riser and cause high interface stresses. *Significance:* This study demonstrated the potential of calcifications in atherosclerotic plaques to cause elevated stresses in plaque tissue and provided a biomechanical explanation for the histopathological findings of calcification-associated plaque rupture.**

***Index Terms*— atherosclerosis, biomechanical stress, calcifications, plaque rupture, morphology**

I. Introduction

THE majority of the cardiovascular events are caused by the rupture of atherosclerotic plaques, which may lead to ischemia in the organs located distally from the plaque [1]–[3]. Histopathological studies on ruptured plaques have identified the presence of a large lipid pool and an overlying thin fibrous cap as the common structural features of unstable plaques [4]–[7]. Plaque stress analysis studies have provided mechanistic explanations for these histology findings by demonstrating that the enlargement of the lipid pool and/or the thinning of the cap may result in elevated plaque stresses [8]–[10], a functional marker of mechanical plaque instability [7], [11], [12].

Another highly prevalent structural component of atherosclerotic plaques is calcification [13]. Contrary to the lipid pool and the fibrous cap, the effects of calcifications on the plaque's mechanical stability is still unclear [14]. Traditionally, calcifications are associated with plaque stability in terms of the link with clinical events, but increasing number of evidence highlights a more complex role for calcification in plaque (in)stability. The histopathological examinations of coronaries have, for example, identified considerable calcification levels in acutely-ruptured and healed plaques [15]. For carotid arteries, higher levels of calcification were significantly associated with a higher incidence of ipsilateral cerebral lesions [16] and hemorrhagic components in the artery [17]. Multiple calcifications were associated with the prevalence of intraplaque hemorrhage, a strong predictor for recurrent stroke [20, 21]. On the other hand, there is also much data suggesting a stabilizing effect for calcifications in

This work was supported in part by the European Commission's Horizon 2020 research and innovation program, under the Marie Skłodowska-Curie grant agreements No. 707404 and No. 749283. Asterisk indicates the corresponding author. (Correspondence to a.akyildiz@erasmusmc.nl).

F.J.H. Gijsen, B Vis and A.C. Akyildiz are with the Department of Biomedical Engineering, Erasmus Medical Center, the Netherlands and the Department of Biomechanical Engineering, Delft University of Technology, Delft, the Netherlands. H.E. Barrett and A.F.W. van der Steen are with the Department of Biomedical Engineering, Erasmus Medical Center, the Netherlands. Amir A. Zadpoor is with the Department of Biomechanical Engineering, Delft University of Technology, Delft, the Netherlands. Hence J. Verhagen is with the Department of Surgery, Erasmus Medical Center, the Netherlands. Daniel Bos is with the Department of Radiology & Nuclear Medicine, and the Department of Epidemiology, Erasmus Medical Center, the Netherlands.

atherosclerosis. For instance, Schuijf *et al.* characterized the majority (~90%) of plaques in stable coronary artery disease as calcified whereas less (~45%) plaques were so in acute coronary syndrome patients [20]. In addition, a systematic review of 24 studies demonstrated a lower degree of plaque calcification in the clinically symptomatic patients as compared to the asymptomatic ones [21].

Biomechanical analysis studies have attempted to explain the abovementioned controversy in clinical findings [14]. Calcifications were shown to reduce the overall plaque tissue stresses due to their relatively greater stiffness and load-bearing capacity as compared to other plaque components [22], [23]. However, stress redistribution in the plaque tissue due to the presence of a calcification might also lead to local high stresses, such as increased cap stresses due to the calcifications located close to the lumen [24], [25]. Local stress concentrations at the interface of micro-calcifications (< 10 μm) were hypothesized to initiate a tear in the plaque tissue, which may propagate to cap rupture [23], [26]. From the mechanical viewpoint, a calcification may act as a stress riser irrespective of its size. Hence, the hypothesis that calcification-mediated stress concentrations in plaque tissue at the calcification interface cause plaque ruptures also applies to larger size (macro-)calcifications. A recent extensive histopathological examination of carotid endarterectomy plaque specimens has provided strong supporting evidence for this, demonstrating that ~45% of the plaque ruptures analyzed were at the interface of a macro-calcification [27].

Another structurally important feature of atherosclerotic plaques is the fibrous tissue architecture. It is well known that the network of collagen, a fibrillar extracellular matrix (ECM) element, is the main load-bearing component in healthy arteries and the arterial mechanical behavior greatly depends on this fiber organization [28]–[30]. Collagen is also abundantly present in atherosclerotic plaque tissue and while being the main component, together with elastin it forms the fibrous ECM network of the plaque [31], [32]. The organization of the fibrillar ECM network in plaque tissue is an important determinant of the mechanical behavior of the plaque tissue [33]. However, data on fiber organization in atherosclerotic plaques is scarce [34]–[36]. Therefore, other than a few recent studies [38] [39], plaque stress analyses do not include fibrous plaque tissue organization, which may have a significant impact on the plaque stress levels and distribution, also at the calcification interface.

The current study aims to provide novel insights into calcification-associated atherosclerotic plaque ruptures in carotid arteries by investigating the mechanics of the plaque tissue-calcification interface. We present a comprehensive morphometric and biomechanical analysis of calcifications in atherosclerotic carotid plaques. Fibrous tissue orientation was implemented in the computational stress analyses and the combined effects of calcification location, morphology, and fiber patterns on the plaque tissue stresses at the calcification interface were analyzed.

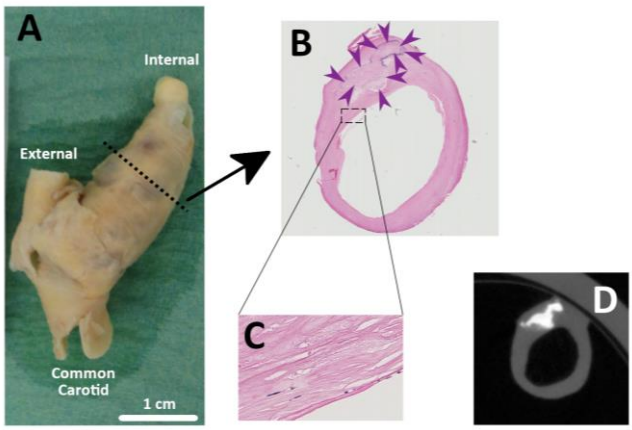

Figure 1: (A) A carotid plaque sample obtained from an endarterectomy surgery, (B) A Hematoxylin & Eosin (H&E) stained histology cross-section. Fibrous plaque tissue has a pale pink color. Calcification is outlined with purple arrowheads. (C) The zoom-in box that shows the detailed fibrous tissue orientation. (D) Micro-computed tomography imaging confirmed the identification of calcifications on histology images. Calcifications can be easily discerned on micro-computed tomography images as white regions.

II. Materials & Methods

A. Plaque samples & histology

Carotid artery plaques were collected from 16 patients (75% male, mean (±SD) age = 69.1 (±7.4)) following endarterectomy surgery at Erasmus Medical Center (Figure 1A). Written informed consent was obtained from all patients, and the study was approved by the local Medical Ethics Committee.

Carotid endarterectomy samples were first fixed with formaldehyde. Then, they were decalcified in a solution of 10% ethylenediaminetetraacetic acid in demineralized water for 14 days and washed in phosphate buffered saline (PBS). The samples were cut in 1 mm thick transversal segments, which were later embedded in paraffin. From each segment, a 5 μm thick section was obtained for histological processing. The acquired sections (n = 335 in total, 21(±4) per plaque specimen on average) were stained histochemically with standard Hematoxylin & Eosin (H&E) stain. H&E staining allowed assessment of fibrous plaque tissue and calcifications in the plaque cross-sections, where the fibrous tissue has a pale pink color and the edge of calcification shows a purple color (Figure 1B and 1C). Stained histological tissue slides were digitized with the NanoZoomer Slide Imaging System (Hamamatsu, Hamamatsu City, Japan) at 40-times magnification.

To obtain a representative set of histology images per plaque sample, every 3rd histology cross-section was selected for further analyses. In total, 112 histological cross sections were included. First, calcifications on the histology cross-sections were identified. The local fiber alignment around the calcifications were analyzed and the calcifications were categorized with regards to the fiber alignment pattern. Four categories of calcifications were identified (Figure 2). The category of 'attached' fiber pattern showed a fibrous tissue architecture around the calcification with a parallel orientation to the radial edges of the calcification (edges parallel to the lumen) and, seemed as if they were "attached" to the

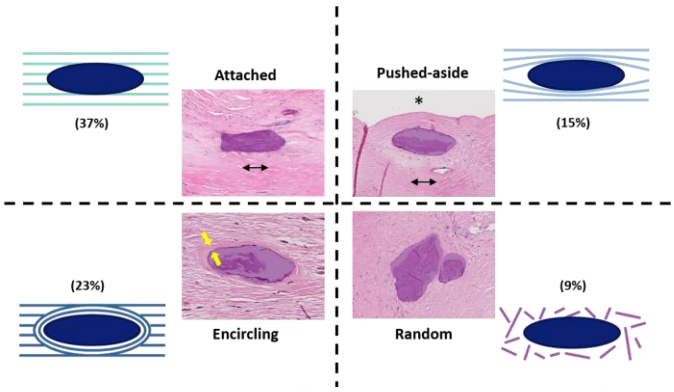

Figure 2: Four distinct patterns of fiber architecture around the calcifications were identified: attached, pushed-aside, encircling and random fiber patterns. Histology examples, corresponding illustrations and prevalence are shown. Double-headed arrows on the histology images indicate the circumferential direction, the black asterisk indicates the lumen and yellow arrowheads the region of encircling fibers. The calcification shapes are highlighted by transparent purple color. The percentages represent the prevalence of each pattern.

calcification at the circumferential edges with an alignment perpendicular to these edges (Figure 2, top left panel). If the fibers were pushed aside by the calcification in the radial direction and there were no fibers attached to the calcification at the circumferential edges, the pattern was labelled as 'pushed-aside' (Figure 2, upper right panel). The 'encircling' category had fibers with an alignment encircling the calcification (Figure 2, lower left panel). In the last category, the 'random' category, the fibers showed random orientation around the calcification (Figure 2, lower right panel).

Subsequently, the size, shape and location of each calcification were identified (Table 1). The first one of the five morphometric features measured was the axial location of a calcification, which was identified by measuring the distance of the histology cross-section from the carotid bifurcation (D_{bif}) (Figure 3A). The other four metrics were obtained by performing measurements on the histology images, which were the distance to the lumen (D_{lum}), the distance to the plaque outer edge (D_{out}), the circumferential arc length (CL), and the radial

TABLE 1:DEFINITIONS OF THE MORPHOMETRIC PARAMETERS

Measurement	***Label***
Calcification distance to the bifurcation	D_{bif}
Calcification distance to the lumen	D_{lum}
Calcification distance to the outer edge	D_{out}
Calcification circumferential length	CL
Calcification radial width	RW

Derived quantity	***Label***	***Definition***
Plaque thickness	Th_{Pl}	$D_{lum} + RW + D_{out}$
Normalized calcification radial location	RL_{norm}	D_{lum} / Th_{Pl}
Calcification aspect ratio	AR	CL / RW
Normalized calcification width	W_{norm}	RW / Th_{Pl}

width (RW) (Figure 3B). From these measurements, the plaque thickness (Th_{pl}) and the normalized morphometric measures of the radial location (RL_{norm}), the aspect ratio (AR), and the normalized width (W_{norm}) were derived for each calcification (Table 1).

B. Biomechanical Analysis

Idealized, complete plaque geometries were used in finite element (FE) models to better mimic the in-vivo loading conditions of a calcification embedded in plaque. For each plaque cross-section with a calcification, a 2D FE model was generated (Figure 3C). The baseline geometry represented an average plaque cross-section of an atherosclerotic carotid artery with geometric dimensions based on the relevant literature [39]–[41]: internal elastic lamina diameter = 5.6 mm, lumen diameter = 2.2 mm, eccentricity index = 0.8 (following the definition of [41]), media thickness = 0.8 mm, and adventitia thickness = 0.27 mm. A calcification with an idealized elliptic shape was placed in the mid-region of the prescribed plaque

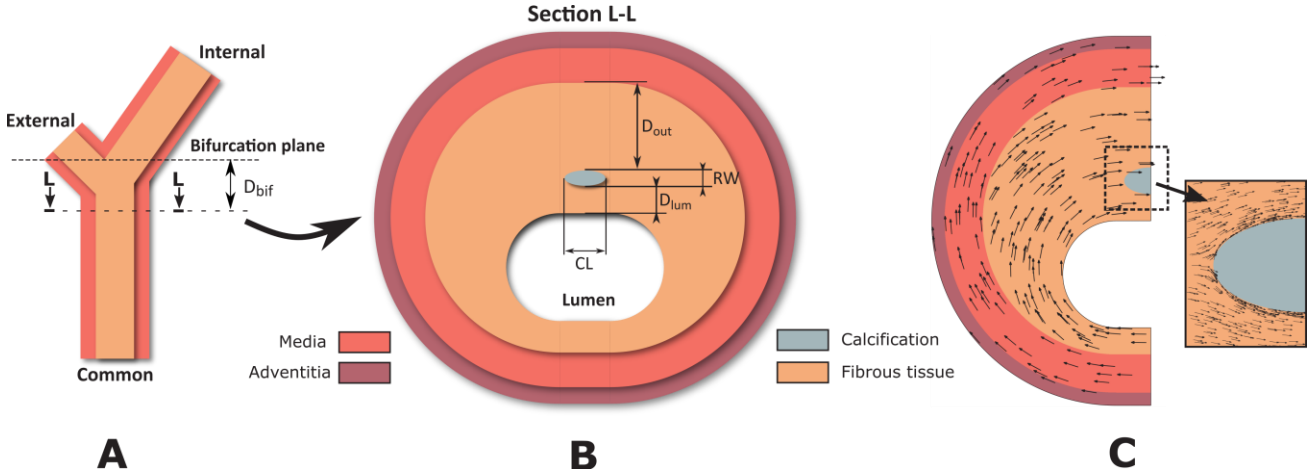

Figure 3: Illustrations of (A) longitudinal cross-section of a carotid artery and (B) a transverse cross-section. Please note that carotid plaques from endarterectomy procedures lack media and adventitia layers. However, these layers are included to illustrate the complete arterial wall. D_{bif} :axial distance of the transverse histology cross-section from the carotid bifurcation. D_{out}: distance of the calcification to the plaque outer edge; RW: calcification radial width; D_{lum}: distance of the calcification to the lumen; and CL: calcification circumferential arc length. (C) A representative geometry for 2D finite element models. The fibrous tissue orientations are indicated with black arrows. The black dotted box shows the subregion in the model, where calcification specific fiber orientation was implemented, in this illustrative case of a pushed-aside fiber pattern.

geometry. The location, size, and geometry of the calcifications were adjusted according to the calcification-specific morphometric measurements of RL_{norm}, AR and W_{norm}, so that a unique FE model for each calcification was generated.

The anisotropic material behavior of the arterial wall layers (adventitia and media) and fibrous plaque tissue was implemented in the FE models by using a hyperelastic model proposed by Gasser *et al.* [42]. The corresponding strain energy density function, W, is described as:

$$W = \frac{\mu}{2}(I_1 - 3) + \frac{k_1}{2k_2}(\exp\{k_2[\kappa(I_1 - 3) + (1 - 3\kappa)(I_4 - 1)^2]\} - 1) \quad (1)$$

where I_1 is the first invariant of the right Cauchy-Green deformation tensor, and $I_4 = (\lambda_{ff} \cos \alpha)^2 + (\lambda_{af} \sin \alpha)^2$ is a pseudo-invariant with λ_{ff} and λ_{af} being respectively the stretch ratios along the fibers (fiber-direction) and transverse to fibers (across-fiber-direction), and α is the local fiber angle in the cross-sectional plane. The parameter $\kappa \in [0, 1/3]$ captures the fiber dispersion, while μ, k_1 & k_2 are the material constants. The material constant values were obtained from the literature [8], [37] (Adventitia: μ = 5.86 kPa, k_1 = 2069.42 kPa, k_2 = 394.28, κ = 0.20; Media: μ = 2.24 kPa, k_1 = 65.76 kPa, k_2 = 76.87, κ = 0.27; Fibrous plaque: μ = 56 kPa, k_1 = 41080 kPa, k_2= 1749.6, κ= 0.136). The relatively stiffer calcification material behavior was prescribed using a linear elastic model, with a Young's modulus of 2 GPa and a Poisson's ratio of 0.49 [43].

A mainly circumferential orientation of fibers, more specifically parallel to the media-adventitia and fibrous tissue-media interfaces, was assumed for the adventitia and media layers in the FE models. For the fibrous plaque tissue, except for the sub-region around the calcification, fibers were aligned circumferentially with respect to the lumen center. The calcification-specific fiber orientation in the plaque tissue around the calcifications was incorporated in the FE models by defining the fiber orientation pattern in a rectangular subregion containing the calcification (Figure 3C, zoom-in box). The width and length of the subregion were set to be 30% larger than the corresponding dimensions of the calcification. For the attached fiber pattern, the fibers in the subregion in the models were aligned in the circumferential direction. The encircling fiber pattern was defined as a layer (a thickness of 0.015 mm as measured in the histology analysis) of fibers around the calcification, where the fiber orientation was parallel to the calcification interface. For random fiber patterns, the dispersion parameter κ in the material model was set to 1/3, resulting in an isotropic material behavior. For the pushed-aside fiber pattern, analytical solutions from the potential flow theory were used to define the fiber orientation [44]. The 2D potential flow field of a horizontal free stream obstructed by an ellipse was solved and the directions of the streamlines were used as the fiber orientations around the calcification.

The obtained model geometries were meshed with quadratic, quadrilateral elements with reduced integration and hybrid formulation. The final size of the elements was obtained from a mesh convergence analysis. The largest element edge dimension was 100 µm and the mesh was locally refined in the regions such as calcification-fibrous tissue interface, where the obtained mesh edge dimension was between 0.2 µm and 2 µm depending on the calcification size and geometry. For the nodes on the symmetry line, only the vertical displacement was allowed and the top node was encastered to prevent rigid body motion. A static intraluminal pressure of 18.7 kPa (140 mmHg) was applied on the plaque lumen surface as loading condition. The FE simulations were performed with ABAQUS/Standard (ver. 2016, DS Simulia, Providence, RI) under plane strain assumption, using quasi-static implicit solver.

With the FE simulations, the following five fibrous plaque tissue stress measures at the calcification-fibrous tissue interface were computed: 1. von Mises stress (σ_{vm}), 2. maximum principal stress (σ_{mp}), 3. fiber-direction stress (σ_{ff}), 4. across-fiber-direction stress (σ_{af}), and 5. fiber-shear stress (σ_{fs}). The fiber-direction stress (σ_{ff}) is defined as the normal stress along the fiber direction, the across-fiber-direction stress (σ_{af}) as the

TABLE 2: QUANTITATIVE MORPHOMETRIC MEASUREMENTS OF CALCIFICATIONS AND PLAQUE ON HISTOLOGY IMAGES. (GRAY-COLORED BOXES INDICATE STATISTICALLY SIGNIFICANT DIFFERENCE ACROSS THE PATTERN GROUPS FOR A GIVEN FEATURE)

		Plaque thickness Th_{Pl} [mm]	Calcification distance to the lumen D_{lum} [mm]	Calcification distance to the outer edge D_{out} [mm]	Calcification circumferential length CL [mm]	Calcification radial width RW [mm]
All (n=145)	Median	2.15	0.96	0.56	0.51	0.24
	Q1 - Q3	1.48-3.04	0.33-2.03	0.21-0.92	0.24-1.22	0.12-0.42
	Min - Max	0.48-6.37	0.01-5.25	0.01-6.10	0.05-3.51	0.04-3.04
Attached (n=64)	Median	2.02	0.44	0.45	1.21	0.34
	Q1 - Q3	1.39-2.65	0.16-1.28	0.12-1.07	0.49-1.77	0.18-0.63
	Min - Max	0.48-6.37	0.01-5.25	0.01-6.10	0.09-3.51	0.07-3.04
Pushed-aside (n=25)	Median	2.05	1.05	0.62	0.45	0.20
	Q1 - Q3	1.67-2.94	0.38-1.45	0.41-1.14	0.27-0.71	0.12-0.35
	Min - Max	0.72-5.87	0.09-4.34	0.14-2.44	0.05-1.36	0.05-0.80
Encircling (n=40)	Median	2.75	1.62	0.78	0.24	0.19
	Q1 - Q3	1.70-3.85	0.69-2.88	0.41-0.97	0.15-0.40	0.11-0.30
	Min - Max	1.17-6.15	0.07-4.18	0.04-5.66	0.05-1.56	0.04-1.14
Random (n=16)	Median	2.19	1.72	0.12	0.27	0.15
	Q1 - Q3	1.84-2.52	1.30-2.12	0.09-0.47	0.13-0.52	0.09-0.29
	Min - Max	0.70-4.61	0.28-4.06	0.06-0.86	0.06-1.26	0.05-0.50

one perpendicular to the fiber direction (transverse direction), and fiber-shear stress (σ_{fs}) defines the shear between the fibers. The stress values were extracted from the fibrous plaque tissue component of the models. The peak values of these stress measures per calcification-fibrous tissue interface are reported as the simulation output. Furthermore, median stress values with the interquartile range [Q1:Q3] are reported for groups.

C. Statistical Analysis

The distributions of the morphometric calcification measures were compared across the calcification groups using non-parametric Kruskal-Wallis H test and a post-hoc pairwise comparison adjusted for the Bonferroni correction for multiple tests. The effects of the calcification size, shape, and location on the peak interfacial plaque tissue stress were studied by the correlation analyses of the normalized morphometric calcification measures (*i.e.*, RL_{norm}, *AR*, and W_{norm}) with the peak stress measures. Due to the non-Gaussian distribution of the data, the non-parametric Spearman's rank-order correlation was used. The threshold of statistical significance was set at $p < 0.05$.

III. Results

A. Calcification and fibrous plaque tissue morphology

Sixty-five out of 112 histological cross sections (58%) contained calcifications. In total, 171 calcifications were identified. For 37% of the calcifications ($n = 64$, observed in 15 patients) the fiber architecture around the calcification was "attached", for 23% of the calcifications ($n = 40$, observed in 12 patients) the fibers were "encircling" the calcification, for 15% of the calcifications ($n = 25$, observed in 10 patients) the fibers were "pushed-aside" and for 9% of the calcifications ($n = 16$, observed in 8 patients) the fibrous tissue showed "random" orientation. The remaining 15% of the calcifications ($n = 26$) demonstrated combinations of these four main patterns.

An examination of the axial distance of the calcifications from the carotid bifurcation, D_{bif}, revealed differences across the patterns. Fifty-six percent of the attached fiber pattern calcifications were located in the internal carotid region and the rest (44%) proximal to the bifurcation point, in the common carotid region. The pushed-aside pattern calcifications showed a similar distribution with 63% of the calcifications in the internal carotid region and 37% in the common carotid region. For the encircling fiber pattern calcifications, there was an even distribution between the internal carotid (50%) and the common carotid region (50%), whereas the random fiber pattern cases were mainly located in the internal carotid artery (94%).

The quantitative morphometric measurements of the calcifications on the histology cross-sections are summarized in Table 2. All plaques considered together, the plaque thickness (Th_{pl}) ranged between 0.48 and 6.37 mm (median = 2.15 mm). The shortest distance of a calcification to the lumen (D_{lum}) was 0.01 mm and the longest was 5.25 mm (median = 0.96 mm). The distance between the calcification and the outer wall (D_{out}) ranged from 0.01 to 6.10 mm (median= 0.56 mm). The circumferential calcification length (*CL*) varied between 0.05 mm and 3.51 mm (median = 0.51 mm) and the radial width (*RW*) was between 0.04 mm and 3.04 mm (median = 0.24 mm). Attached fiber pattern calcifications were located statistically significantly closer to the lumen than the other three patterns (median D_{lum} = 0.44 mm vs. 1.05 mm for pushed-aside, 1.62 mm for encircling, and 1.72 mm for random). The random fiber pattern calcifications had significantly shorter distance to the plaque outer edge, D_{out} (median = 0.12 mm vs. 0.45 mm for attached, 0.62 mm for pushed-aside, and 0.78 mm for encircling). Moreover, the attached fiber pattern calcifications showed significantly larger circumferential lengths, *CL* (median = 1.21 mm vs. 0.45 mm for pushed-aside, 0.24 mm for encircling, and 0.27 mm for random) and radial width, *RW* (median = 0.34 mm vs. 0.20 mm for pushed-aside, 0.19 mm for encircling, and 0.15 mm for random).

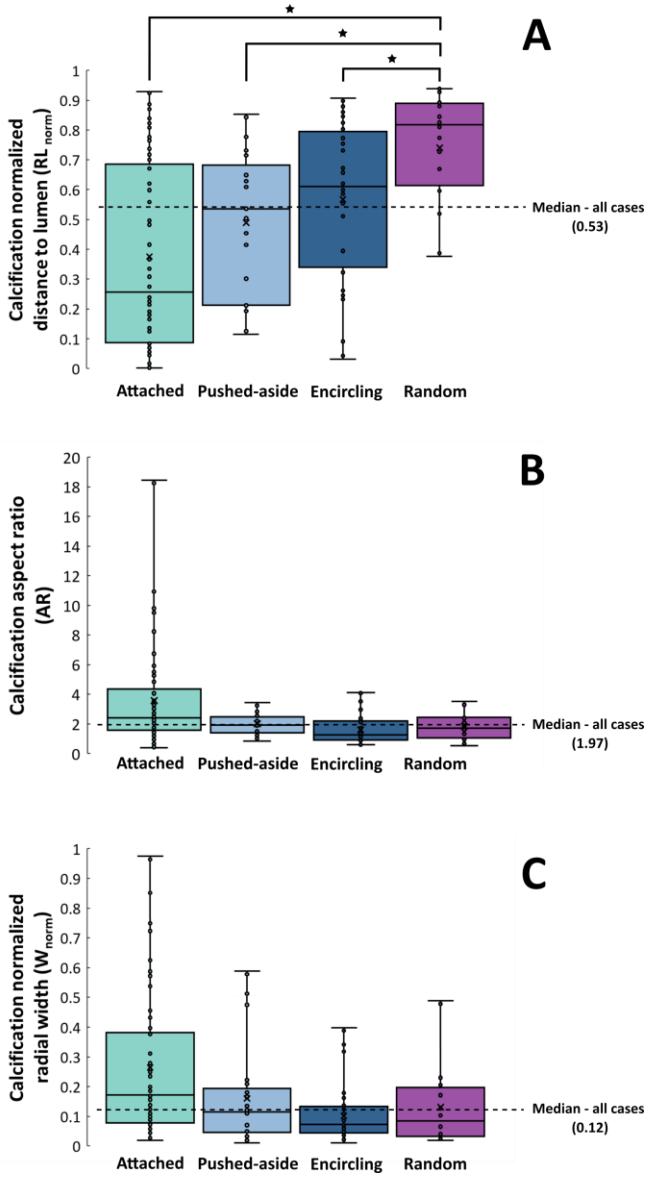

Figure 4: Distribution of the normalized morphometric features of carotid plaque calcifications classified according to fiber pattern: A) normalized radial location (RL_{norm}), B) aspect ratio (AR) and C) normalized width (W_{norm}). The boxplots indicate median, 1st and 3rd quartiles, and the range. Statistically significant differenced across patterns are indicated by a star symbol.

Figure 4 demonstrates the distribution of the three normalized morphometric features per fiber pattern group. Attached fiber pattern calcifications showed the largest range for all three normalized morphometric features. The normalized distance to the lumen (RL_{norm}) of the attached group had a range between 0.01 and 0.93 and a median of 0.26 (Figure 4*A*). The calcifications of the other three fiber patterns were located further away from the lumen. The random fiber pattern group demonstrated a statistically significant greater distance from the lumen than the other three patterns with a median RL_{norm} of 0.86. The median aspect ratios (*AR*) of the calcifications (Figure 4*B*) were greater than 1 for all four fiber patterns (2.41 for attached, 1.92 for pushed-aside, 1.26 for encircling, and 1.71 for random pattern). This implies that the calcifications had mainly slender shapes with the major axis aligned in the circumferential direction as an *AR* equal to unity means equal dimensions in both circumferential and radial directions. Fifteen attached fiber pattern calcifications had an aspect ratio >5, implying a very slender calcification shape. The median normalized radial width (W_{norm}) values (Figure 4*C*) were 0.17 for the attached fiber pattern group, 0.11 for the pushed-aside, 0.07 for the encircling, and 0.08 for the random. Some calcifications, especially in the attached fiber group, had large W_{norm} values.

B. Fibrous plaque tissue stresses at calcification interface

Figure 5 demonstrates the von Mises stress distribution in a representative plaque model (RL_{norm} = 0.15, *AR* = 3.9, and W_{norm} = 0.12, attached fiber pattern) with a stress concentration in the fibrous plaque tissue at the calcification interface. Overall, the von Mises stresses in the fibrous plaque tissue showed low values (< 5 kPa). However, the presence of the calcification caused stress concentration at the calcification interface with a peak stress value of 585 kPa. This peak interface stress was the highest in the entire plaque tissue, in this case 34% higher than the maximum von Mises stress at the lumen (435 kPa). This illustrative case, valid for the specified geometry and material properties, demonstrate the likelihood of high stresses at calcification interfaces.

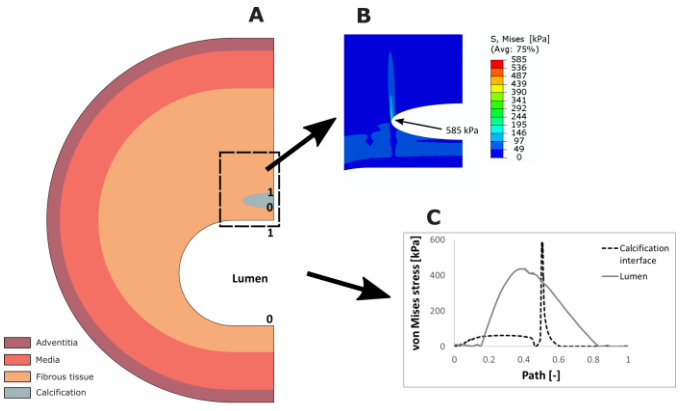

Figure 5: (A) A representative finite element model of the attached fiber pattern with RL_{norm} = 0.15, AR = 3.9 and W_{norm} = 0.12, and (B) the corresponding von Mises stress distribution in the fibrous plaque tissue around the calcification. (C) the von Mises stress distribution along the calcification interface path and lumen path. The path start point (0) and end point (1) are indicated in the model (A) for both the lumen and the calcification interface. The maximum plaque tissue stress is 585 kPa and located at the calcification-tissue interface, whereas the highest stress at the lumen is 435 kPa.

Figure 6 presents the distribution of the computed peak stress measures per fiber pattern group, except for the maximum principal stress. For all the plaque models, the maximum principal interface stress values, σ_{mp} correlated significantly (R^2 = 0.96) with the fiber-direction interface stresses, σ_{ff}. Therefore, σ_{mp} is not separately reported. The attached fiber pattern calcifications showed peak von Mises interface stresses, σ_{vm} with a median [Q1-Q3] of 415 [236:811] kPa (Figure 6A). Eleven cases reached stress values greater than 1 MPa. The pushed-aside fiber pattern group showed lower peak von Mises interface stresses with a median of 128 [63:242] kPa. The peak von Mises interface stresses for the encircling pattern and random fiber pattern groups were much lower, with a median of 8 [4:31] kPa for the encircling and 4 [2:8] kPa for the random fiber pattern group.

Generally, the peak fiber-direction interface stresses, σ_{ff} (Figure 6B) were lower than the von Mises stresses, σ_{vm} (Figure 6A). Among the groups, the pushed-aside fiber pattern group demonstrated the highest stresses, with a median of 111 [67:196] kPa, followed by the attached fiber pattern group with a median of 42 [14:72] kPa. The encircling pattern presented much lower stresses (median of 5 [2:17] kPa). Due to the uniform fiber distribution for the random fiber pattern group, the fiber-direction interface stresses, $\sigma_{ff,}$ across-fiber-direction interface stresses, σ_{af}, and fiber-shear interface stresses, σ_{fs}, could not be defined. Hence, the maximum principal stress, σ_{mp} is reported instead of the fiber-direction interface stresses, $\sigma_{ff,}$ in Figure 6B and the corresponding values are missing in Figure 6C and 6D for the random fiber pattern group.

The peak across-fiber-direction interface stresses, σ_{af} (Fig. 6C) were lower than the von Mises, σ_{vm}, and fiber-direction interface stresses, σ_{ff}, for all fiber pattern groups. The median was 16 [8:40] kPa for the attached fiber pattern group and 12 [4:21] kPa for the pushed-aside group. The encircling fiber pattern group presented the lowest peak across-fiber-direction interface stresses with a median value smaller than 10 kPa. The encircling and pushed-aside fiber pattern groups showed also very low peak fiber-shear interface stresses, σ_{fs} (median values < 10 kPa) (Figure 6D). The attached pattern had the highest peak fiber-shear stresses with a median of 45 [21: 92] kPa. The maximum value for this pattern group was 690 kPa.

C. Impact of calcification morphology on interface stresses

Table 3 presents the Spearman's rank-order correlation coefficients (ρ) between the normalized morphometric measures (RL_{norm}, *AR*, and W_{norm}) and the peak interfacial plaque tissue stress measures (σ_{vm}, σ_{ff}, σ_{fs}, and σ_{af}) per pattern and for all cases pooled, where the correlations with a statistical significance of $p < 0.05$ are highlighted in gray color. When all calcification patterns were combined, all three morphometric measures showed statistically significant correlations with the stress measures. RL_{norm} demonstrated a negative correlation,

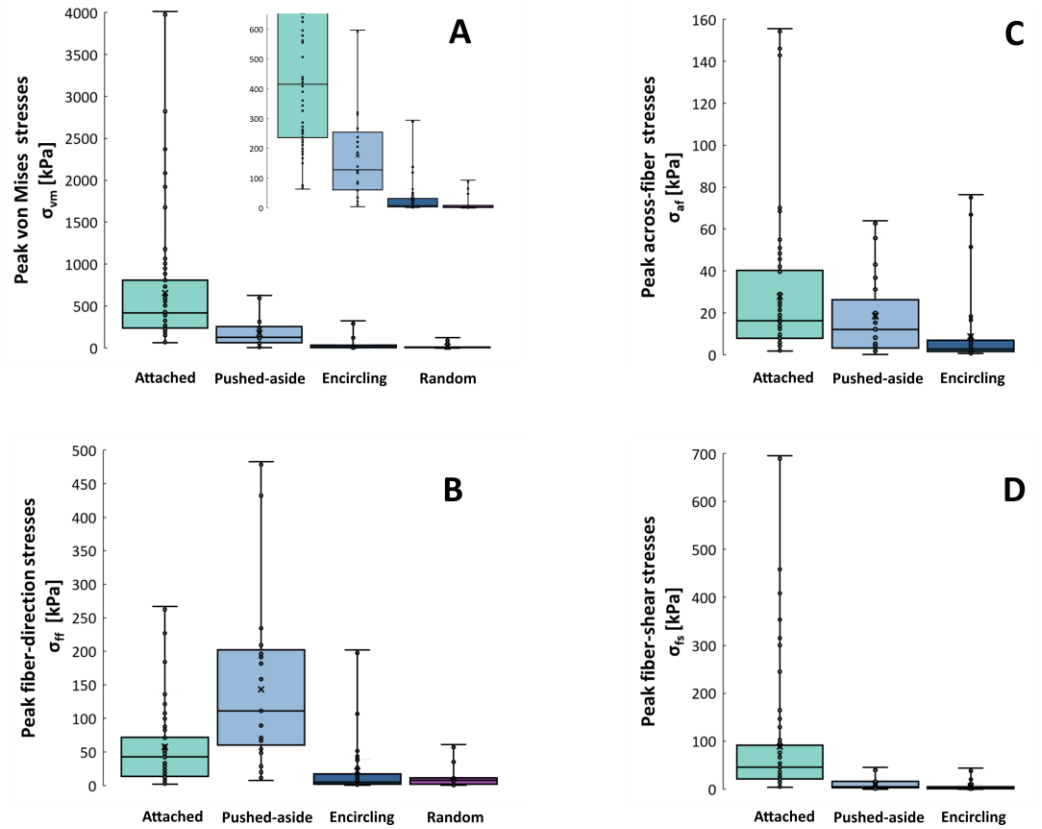

Figure 6: Peak von Misses (A), fiber-direction (B), across-fiber-direction (C) and fiber-shear (D) stresses of the fibrous plaque tissue at the calcification interface per fibrous tissue pattern group. The boxplots indicate median, 1st and 3rd quartiles, and the range. Each dot represents the peak interface stress value of a finite element model. The close-up box in A is to provide more detailed information about the groups with relatively lower values. (Please note that the maximum principal stress σ_{mp} is reported instead of the fiber-direction interface stresses σ_{ff} for the random fiber pattern in B.)

and *AR* and W_{norm} positive correlation with the stress measures. The correlations were moderate in the case of RL_{norm} and W_{norm} ($|\rho|$ = [0.28-0.53]) but stronger in the case of *AR* (ρ = [0.57-0.67]).

When the individual fiber pattern groups were analyzed separately, the signs (positivity or negativity) of the correlations were the same as in the case of all calcification cases combined. For the attached fiber pattern calcifications, *AR* was the only morphometric measure with a statistical significance and had moderate to strong correlations with the stress measures (ρ = [0.55-0.78]). For the pushed-aside group, RL_{norm} had a strong correlation with the stress measures ($|\rho|$ = [0.64-0.75]). *AR* and W_{norm} showed lower correlations, and only with two stress measures (σ_{vm} and σ_{af}). For the encircling group, *AR* showed strong correlations (ρ = [0.74-0.76]) with all the stress measures except σ_{af}. Low to moderate correlations ($|\rho|$ = [0.27-0.75]) were observed for RL_{norm} and W_{norm} in this group. For the random pattern group, *AR* and W_{norm} showed moderate to strong correlations with the stress measures (ρ = [0.66-0.69]).

IV. Discussion

We studied the effects of arterial calcifications on the stress distribution in the fibrous plaque tissue at the calcification interface, as a potential source of plaque rupture in carotid arteries and clinical cerebrovascular events. The study involved a comprehensive morphometric analysis of carotid artery calcification, a mechanical analysis of the stresses at the calcification - fibrous plaque tissue interface, and an analysis of the correlations between calcification morphology and plaque tissue fiber organization on the one hand and the interface stresses on the other.

Table 3: Spearman's rank-order correlation coefficient (ρ) with a statistical significance of $p < 0.05$ between the normalized morphometric measures (RL_{norm}, AR and W_{norm}) and the peak interfacial plaque tissue stress measures. (Gray-colored boxes indicate statistically significant correlations.)

		RL_{norm}	AR	W_{norm}
All	σ_{vm}	-0.49	0.67	0.46
	σ_{ff}	-0.41	0.57	0.31
	σ_{fs}	-0.40	0.67	0.28
	σ_{af}	-0.51	0.64	0.53
Attached	σ_{vm}	-0.16	0.78	0.01
	σ_{ff}	-0.23	0.55	-0.11
	σ_{fs}	-0.13	0.72	-0.24
	σ_{af}	-0.21	0.70	0.02
Pushed-aside	σ_{vm}	-0.73	0.44	0.57
	σ_{ff}	-0.71	0.35	0.60
	σ_{fs}	-0.64	0.25	0.25
	σ_{af}	-0.75	0.42	0.57
Encircling	σ_{vm}	-0.50	0.76	0.43
	σ_{ff}	-0.44	0.74	0.39
	σ_{fs}	-0.40	0.74	0.27
	σ_{af}	-0.65	0.44	0.75
Random	σ_{vm}	-0.37	0.69	0.69
	σ_{mp}	-0.36	0.66	0.68

The morphometric analysis provided unique information about the size, location, and geometrical features of carotid plaque calcifications, and about the fiber organization in the plaque tissue surrounding the calcifications. The study results showed that carotid plaque calcifications are generally aligned in the circumferential direction and demonstrate large variations in size, shape, and location. Four distinct fiber organization patterns around the calcifications were identified, termed as attached, pushed-aside, encircling, and random. The attached fiber pattern was the most prevalent one and the random fiber pattern was observed least frequently.

The calcifications in the attached fiber pattern group were located close to the lumen, sometimes as close as few tens of micrometers. These calcifications were generally thicker in the radial direction and longer in the circumferential direction. Furthermore, they had the largest variation in the geometrical features. The attached fiber pattern calcification was distinct from the other three groups with the fiber alignment being not disrupted. The fiber structure was still visible inside the calcifications on the histology images. This possibly indicates that this type of calcifications develops due to the fiber mineralization, which also explains the slender shape, with aspect ratios as large as 18. This type of calcification process is associated with bone formation in plaques [45], that is related to an active pathway that involves osteoblast- and osteoclast-like cells that are present in the more advanced stages of atherosclerosis [46], [47]. The other three organization patterns did not show any signs of fiber structure inside, indicating that they might be formed through the agglomeration of extracellular vesicles and apoptotic cells [13]. The pushed-aside and encircling pattern were evenly distributed in the radial direction, but the random fiber pattern calcifications were mainly located in the internal carotid artery, closer to the outer wall. A possible explanation for the findings on the distinct location of the attached and random fiber pattern calcifications is that fibers close to the lumen are well organized and are aligned in parallel to the lumen, whereas the fibers deeper in the plaque tissue do not demonstrate such a clear structural organization [37].

The stress analyses showed that the calcifications, particularly with the attached or pushed-aside fiber pattern, can lead to elevated von Mises and fiber-direction stresses at the interface. For some calcifications, these stresses reached values higher than the strength values reported for the plaque tissue [48], [49]. Our numerical results support the hypothesis that a rupture in a plaque may start at a calcification interface, a possible explanation for the histopathological findings of plaque ruptures associated with the presence of calcifications [27]. The across-fiber-direction and fiber-shear stress values were generally much lower than von Mises and fiber-direction stresses. Notwithstanding, at the interface of calcifications with the attached fiber pattern, high values for across-fiber-direction and fiber-shear stress values were observed. The fact that the across-fiber-direction and fiber-shear stress values were lower does not mean that they are not relevant when considering interface failure, since the plaque strength levels associated with failure in the shear mode are unknown. For such failure modes, the strength values associated with the cross-links between the fibers are likely to be more important than the strength values of the fibers [27], [37]. In the anisotropic fibrous plaque tissue, the main load-bearing component is the fibers. Therefore, there was an almost perfect correlation between von Mises and maximum principal stresses.

Overall, thicker calcifications of a circumferentially slender shape that are close to the lumen showed higher peak interfacial stresses. Having greater thickness and being located closer to the lumen predispose the luminal side of the calcification interface to this relatively higher stress region of the plaque, where this base level stresses are even further amplified by the stress-concentration effects of the calcification. Moreover, the calcifications are subjected to stresses due to the bending moments experienced during the intraluminal pressurization of the atherosclerotic vessel, which increase with the aspect ratio. With regards to the different fiber orientation patterns, the influence of radial location on stress results was not significant for the attached pattern. The calcifications with this fiber pattern were often so slender that the aspect ratio dominated all other features. The influence of the normalized radial location was not significant for the random pattern either, since these calcifications were mostly located near the outer wall. The normalized aspect ratio showed the most consistent relationship for all fiber pattern groups with the interface stresses: long, slender calcifications, regardless of their location and fiber pattern, led to interface stress concentrations. This was especially true for the attached pattern, which did not demonstrate statistically significant impact of normalized radial location and width on stress measures.

This study also illustrates that the impact of calcifications on plaque stability cannot be explained by solely a single factor, such as the presence of calcification or its area but depends on multiple factors. Previous studies have demonstrated that calcifications lower the cap stresses and this effect is further amplified as the calcification size increases. That is because the calcification with a stiffness greater than the fibrous tissue carries larger portion of the load exerted by the lumen pressure [14], [22]. However, the current study clearly showed that a calcification can also act as a stress riser and the calcification-fibrous tissue interface is exposed to high stress. We also found that the complex interplay between the location and shape determines the interface stresses. Advanced computational tools, such as FE models are, therefore, required for any quantitative analysis.

Although in this study the choice of the FE models of full plaque cross-sections was not made to analyze the overall plaque stresses, but to only provide with more relevant and accurate boundary conditions for the stress computations of the fibrous tissue-calcification interface, they did provide us with a means to qualitatively compare the interface stresses at the calcifications with luminal stress values. In some cases, the interface stress exceeded the stress values at the luminal border. Although stress levels at the lumen are influenced by the local curvature [8], and the failure mechanisms at the lumen are potentially different from the ones at the fibrous tissue - calcification interface within a plaque [29,38], the results from

this study support the hypothesis that, in some cases, plaque rupture might originate from initiating tears at the interface and not at the luminal side [29], especially when slender calcifications are located close to the lumen.

The current study has some limitations. It is worth to mention that we focused on the interfacial stresses of a single calcification in a plaque. In practice, plaques can contain multiple calcifications. The impact of the presence of another calcification or a compliant lipid pool in the proximity of a calcification on the interface stresses warrants future research. Secondly, although each calcification geometry was generated based on real histological measurements, the calcification geometries for the FE analyses were simplified and idealized with elliptic shapes. This prevented studying the potential effects of, for instance, the local calcification curvature at the interface on the generated stresses. Thirdly, H&E staining is a general staining, widely used for identification of the macroscopic atherosclerotic plaque components, including fibrous extracellular matrix (ECM) and calcification [27], [37], [50]–[53]. However, H&E is not specific for any ECM protein. The fibrous tissue of atherosclerotic plaques mainly consists of collagen and elastin, and it was previously shown that the collagen:elastin ratio in plaques are 7:1 [32]. Therefore, the fibrous tissue identified in our study by H&E staining is likely to be predominantly collagen, yet conclusive information on this requires collagen and elastin specific histology stainings. Moreover, the stress analyses were performed with 2D computational models based on the data obtained from histology since the 3D, high resolution morphometric information required for the 3D computations was not available. The 3D geometry of the calcifications can be obtained using micro-CT imaging; however, to our best knowledge, there are no means of obtaining the 3D fiber orientation in the fibrous plaque tissue in high resolution for sufficiently large volumes. In this regard, pre-clinical DT-MRI imaging holds a potential [36], but the technique still requires some advancement to provide high resolution data. Although 3D computational models may result in slightly different stress results, we do not expect the main conclusions of the current study to change. Due to the scarcity of the anisotropic material behavior data of the atherosclerotic artery layers, we used data for coronary arteries with intimal thickening for the media and adventitia layers. Furthermore, we used in the computational models a fixed stiffness value (2GPa) for calcium, which corresponds to the high regime of the values reported by Ebenstein et al. [43]. Although these authors reported stiffness values that span a few orders of magnitude, they stated that their low stiffness indentation measurements are possibly due to the fibrous tissue fragments remained attached to the calcifications and the fully mineralized calcifications are likely to have a stiffness in the order of GPa. In this regard, the calcifications in our models should be considered as fully mineralized. Furthermore, Cahalane et al. [54] recently reported calcium stiffness values between 17-25 GPa. A sensitivity analysis in a randomly selected small subgroup (n=10) of our models showed <1% change in stress when calcium stiffness was increased to 20 GPa. The histological imaging data used in this study provided only limited information on the physical nature of the contact between the fibrous tissue and the calcifications. Although previous studies, including scanning electron imaging [55] indicated a direct contact between the collagen fibers and the calcification, we could not establish such interactions based on imaging data available in the data-set used in the current study. The interaction between the fibrous tissue is of great importance, especially in the context of plaque failure and plaque stability [14]; therefore, warrants further research.

V. Conclusion

The current study demonstrated the large degree of variation in the shape, size, and location of plaque calcifications, in addition to the fibrous tissue architecture around the calcifications. Thicker calcifications with a circumferential slender shape that are close to the lumen showed higher plaque stresses at the calcification interface. The impact of these calcification geometric features was modulated by the fiber organization around the calcification. Plaque tissue stresses at the calcification interfaces can reach stresses higher than the lumen stresses and the reported plaque strength values. This provides a mechanical explanation for the histopathological findings of plaque ruptures associated with calcifications.

References

[1] H. Jia *et al.*, "In Vivo Diagnosis of Plaque Erosion and Calcified Nodule in Patients With Acute Coronary Syndrome by Intravascular Optical Coherence Tomography," *Journal of the American College of Cardiology*, vol. 62, no. 19, pp. 1748–1758, Nov. 2013, doi: 10.1016/j.jacc.2013.05.071.

[2] L. G. Spagnoli *et al.*, "Extracranial Thrombotically Active Carotid Plaque as a Risk Factor for Ischemic Stroke," *JAMA*, vol. 292, no. 15, pp. 1845–1852, Oct. 2004, doi: 10.1001/jama.292.15.1845.

[3] K. Yahagi, H. R. Davis, E. Arbustini, and R. Virmani, "Sex differences in coronary artery disease: Pathological observations," *Atherosclerosis*, vol. 239, no. 1, pp. 260–267, Mar. 2015, doi: 10.1016/j.atherosclerosis.2015.01.017.

[4] E. Falk, "Pathogenesis of Atherosclerosis," *Journal of the American College of Cardiology*, vol. 47, no. 8, pp. C7–C12, Apr. 2006, doi: 10.1016/j.jacc.2005.09.068.

[5] R. Virmani, A. P. Burke, A. Farb, and F. D. Kolodgie, "Pathology of the Vulnerable Plaque," *Journal of the American College of Cardiology*, vol. 47, no. 8, pp. C13–C18, Apr. 2006, doi: 10.1016/j.jacc.2005.10.065.

[6] S. Carr, A. Farb, W. H. Pearce, R. Virmani, and J. S. T. Yao, "Atherosclerotic plaque rupture in symptomatic carotid artery stenosis," *Journal of Vascular Surgery*, vol. 23, no. 5, pp. 755–766, May 1996, doi: 10.1016/S0741-5214(96)70237-9.

[7] J. Schaar, "Terminology for high-risk and vulnerable coronary artery plaques," *European Heart Journal*, vol. 25, no. 12, pp. 1077–1082, Jun. 2004, doi: 10.1016/j.ehj.2004.01.002.

[8] A. C. Akyildiz *et al.*, "Effects of intima stiffness and plaque morphology on peak cap stress," *BioMedical*

Engineering OnLine, vol. 10, no. 1, p. 25, 2011, doi: 10.1186/1475-925X-10-25.

[9] A. C. Akyildiz *et al.*, "The effects of plaque morphology and material properties on peak cap stress in human coronary arteries," *Computer Methods in Biomechanics and Biomedical Engineering*, vol. 19, no. 7, pp. 771–779, May 2016, doi: 10.1080/10255842.2015.1062091.

[10] J. Ohayon *et al.*, "Necrotic core thickness and positive arterial remodeling index: emergent biomechanical factors for evaluating the risk of plaque rupture," *American Journal of Physiology-Heart and Circulatory Physiology*, vol. 295, no. 2, pp. H717–H727, Aug. 2008, doi: 10.1152/ajpheart.00005.2008.

[11] G. C. Cheng, H. M. Loree, R. D. Kamm, M. C. Fishbein, and R. T. Lee, "Distribution of circumferential stress in ruptured and stable atherosclerotic lesions. A structural analysis with histopathological correlation.," *Circulation*, vol. 87, no. 4, pp. 1179–1187, Apr. 1993, doi: 10.1161/01.CIR.87.4.1179.

[12] P. Richardson, "Influence of Plaque Configuration And Stress Distribution on Fissuring of Coronary Atherosclerotic Plaques," *The Lancet*, vol. 334, no. 8669, pp. 941–944, Oct. 1989, doi: 10.1016/S0140-6736(89)90953-7.

[13] R. Virmani, F. D. Kolodgie, A. P. Burke, A. Farb, and S. M. Schwartz, "Lessons From Sudden Coronary Death: A Comprehensive Morphological Classification Scheme for Atherosclerotic Lesions," *Arteriosclerosis, Thrombosis, and Vascular Biology*, vol. 20, no. 5, pp. 1262–1275, May 2000, doi: 10.1161/01.ATV.20.5.1262.

[14] H. E. Barrett, K. Van der Heiden, E. Farrell, F. J. H. Gijsen, and A. C. Akyildiz, "Calcifications in atherosclerotic plaques and impact on plaque biomechanics," *Journal of Biomechanics*, vol. 87, pp. 1–12, Apr. 2019, doi: 10.1016/j.jbiomech.2019.03.005.

[15] A. P. Burke, A. Taylor, A. Farb, G. T. Malcolm, and R. Virmani, "Coronary calcification: insights from sudden coronary death victims," *Zeitschrift fur Kardiologie*, vol. 89, no. 14, pp. S049–S053, Feb. 2000, doi: 10.1007/s003920070099.

[16] R. Pini *et al.*, "Relationship between Calcification and Vulnerability of the Carotid Plaques," *Annals of Vascular Surgery*, vol. 44, pp. 336–342, Oct. 2017, doi: 10.1016/j.avsg.2017.04.017.

[17] Q. J. A. van den Bouwhuijsen *et al.*, "Coexistence of Calcification, Intraplaque Hemorrhage and Lipid Core within the Asymptomatic Atherosclerotic Carotid Plaque: The Rotterdam Study," *CED*, vol. 39, no. 5–6, pp. 319–324, 2015, doi: 10.1159/000381138.

[18] Lin Ruolan, Chen Shuo, Liu Gaifen, Xue Yunjing, and Zhao Xihai, "Association Between Carotid Atherosclerotic Plaque Calcification and Intraplaque Hemorrhage," *Arteriosclerosis, Thrombosis, and Vascular Biology*, vol. 37, no. 6, pp. 1228–1233, Jun. 2017, doi: 10.1161/ATVBAHA.116.308360.

[19] J. Yang *et al.*, "Superficial and multiple calcifications and ulceration associate with intraplaque hemorrhage in the carotid atherosclerotic plaque," *Eur Radiol*, vol. 28, no. 12, pp. 4968–4977, Dec. 2018, doi: 10.1007/s00330-018-5535-7.

[20] J. D. Schuijf *et al.*, "Differences in plaque composition and distribution in stable coronary artery disease versus acute coronary syndromes; non-invasive evaluation with multi-slice computed tomography," *Acute Cardiac Care*, vol. 9, no. 1, pp. 48–53, Jan. 2007, doi: 10.1080/17482940601052648.

[21] R. M. Kwee, "Systematic review on the association between calcification in carotid plaques and clinical ischemic symptoms," *Journal of Vascular Surgery*, vol. 51, no. 4, pp. 1015–1025, Apr. 2010, doi: 10.1016/j.jvs.2009.08.072.

[22] H. Huang, R. Virmani, H. Younis, A. P. Burke, R. D. Kamm, and R. T. Lee, "The Impact of Calcification on the Biomechanical Stability of Atherosclerotic Plaques," *Circulation*, vol. 103, no. 8, pp. 1051–1056, Feb. 2001, doi: 10.1161/01.CIR.103.8.1051.

[23] Y. Vengrenyuk, L. Cardoso, and S. Weinbaum, "Micro-CT Based Analysis of a New Paradigm for Vulnerable Plaque Rupture: Cellular Microcalcifications in Fibrous Caps," p. 12, 2008.

[24] Zhongzhao Teng *et al.*, "How Does Juxtaluminal Calcium Affect Critical Mechanical Conditions in Carotid Atherosclerotic Plaque? An Exploratory Study," *IEEE Transactions on Biomedical Engineering*, vol. 61, no. 1, pp. 35–40, Jan. 2014, doi: 10.1109/TBME.2013.2275078.

[25] Z.-Y. Li, S. Howarth, T. Tang, M. Graves, J. U-King-Im, and J. H. Gillard, "Does Calcium Deposition Play a Role in the Stability of Atheroma? Location May Be the Key," *Cerebrovascular Diseases*, vol. 24, no. 5, pp. 452–459, 2007, doi: 10.1159/000108436.

[26] L. Cardoso and S. Weinbaum, "Changing Views of the Biomechanics of Vulnerable Plaque Rupture: A Review," *Annals of Biomedical Engineering*, vol. 42, no. 2, pp. 415–431, Feb. 2014, doi: 10.1007/s10439-013-0855-x.

[27] M. J. Daemen *et al.*, "Carotid plaque fissure: An underestimated source of intraplaque hemorrhage," *Atherosclerosis*, vol. 254, pp. 102–108, Nov. 2016, doi: 10.1016/j.atherosclerosis.2016.09.069.

[28] P. Fratzl, Ed., *Collagen: Structure and Mechanics*. Springer US, 2008.

[29] G. A. Holzapfel, "Collagen in Arterial Walls: Biomechanical Aspects," in *Collagen: Structure and Mechanics*, P. Fratzl, Ed. Boston, MA: Springer US, 2008, pp. 285–324.

[30] J. D. Humphrey, *Cardiovascular Solid Mechanics: Cells, Tissues, and Organs*. New York: Springer-Verlag, 2002.

[31] M. D. Rekhter, "Collagen synthesis in atherosclerosis: too much and not enough," *Cardiovasc Res*, vol. 41, no. 2, pp. 376–384, Feb. 1999, doi: 10.1016/S0008-6363(98)00321-6.

[32] B. Rokosova and J. P. Bentley, "Composition and metabolism of symptomatic distal aortic plaque," *Journal of Vascular Surgery*, vol. 3, no. 4, p. 6, 1986.

[33] C.-K. Chai *et al.*, "Local anisotropic mechanical properties of human carotid atherosclerotic plaques –

Characterisation by micro-indentation and inverse finite element analysis," *Journal of the Mechanical Behavior of Biomedical Materials*, vol. 43, pp. 59–68, Mar. 2015, doi: 10.1016/j.jmbbm.2014.12.004.

[34] Deguchi Jun-O *et al.*, "Matrix Metalloproteinase-13/Collagenase-3 Deletion Promotes Collagen Accumulation and Organization in Mouse Atherosclerotic Plaques," *Circulation*, vol. 112, no. 17, pp. 2708–2715, Oct. 2005, doi: 10.1161/CIRCULATIONAHA.105.562041.

[35] B. V. Shekhonin, S. P. Domogatsky, V. R. Muzykantov, G. L. Idelson, and V. S. Rukosuev, "Distribution of Type I, III, IV and V Collagen in Normal and Atherosclerotic Human Arterial Wall: Immunomorphological Characteristics," *Collagen and Related Research*, vol. 5, no. 4, pp. 355–368, Sep. 1985, doi: 10.1016/S0174-173X(85)80024-8.

[36] A. C. Akyildiz *et al.*, "3D Fiber Orientation in Atherosclerotic Carotid Plaques," *Journal of Structural Biology*, vol. 200, no. 1, pp. 28–35, Oct. 2017, doi: 10.1016/j.jsb.2017.08.003.

[37] G. R. Douglas, A. J. Brown, J. H. Gillard, M. R. Bennett, M. P. F. Sutcliffe, and Z. Teng, "Impact of Fiber Structure on the Material Stability and Rupture Mechanisms of Coronary Atherosclerotic Plaques," *Annals of Biomedical Engineering*, vol. 45, no. 6, pp. 1462–1474, Jun. 2017, doi: 10.1007/s10439-017-1827-3.

[38] A. C. Akyildiz, F. J. H. Gijsen, and D. Rutten, "Mechanical Predictors of Atherosclerotic Plaque Rupture: Beyond 'Where Stress, There Rupture,'" in *Book of Abstracts of the 25th Congress of the European Society of Biomechanics (ESB 2019)*, Vienna, Austria, 2019, p. 95.

[39] Wong M, Edelstein J, Wollman J, and Bond M G, "Ultrasonic-pathological comparison of the human arterial wall. Verification of intima-media thickness.," *Arteriosclerosis and Thrombosis: A Journal of Vascular Biology*, vol. 13, no. 4, pp. 482–486, Apr. 1993, doi: 10.1161/01.ATV.13.4.482.

[40] Krejza Jaroslaw *et al.*, "Carotid Artery Diameter in Men and Women and the Relation to Body and Neck Size," *Stroke*, vol. 37, no. 4, pp. 1103–1105, Apr. 2006, doi: 10.1161/01.STR.0000206440.48756.f7.

[41] T. Ohara *et al.*, "Eccentric Stenosis of the Carotid Artery Associated with Ipsilateral Cerebrovascular Events," *American Journal of Neuroradiology*, vol. 29, no. 6, pp. 1200–1203, Jun. 2008, doi: 10.3174/ajnr.A0997.

[42] T. C. Gasser, R. W. Ogden, and G. A. Holzapfel, "Hyperelastic modelling of arterial layers with distributed collagen fibre orientations," *Journal of The Royal Society Interface*, vol. 3, no. 6, pp. 15–35, Feb. 2006, doi: 10.1098/rsif.2005.0073.

[43] D. M. Ebenstein, D. Coughlin, J. Chapman, C. Li, and L. A. Pruitt, "Nanomechanical properties of calcification, fibrous tissue, and hematoma from atherosclerotic plaques," *Journal of Biomedical Materials Research Part A*, vol. 91A, no. 4, pp. 1028–1037, Dec. 2009, doi: 10.1002/jbm.a.32321.

[44] F. White, *Fluid Mechanics*, 8 edition. New York, NY: McGraw-Hill Education, 2015.

[45] Hunt Jennifer L. *et al.*, "Bone Formation in Carotid Plaques," *Stroke*, vol. 33, no. 5, pp. 1214–1219, May 2002, doi: 10.1161/01.STR.0000013741.41309.67.

[46] A. P. Sage, Y. Tintut, and L. L. Demer, "Regulatory mechanisms in vascular calcification," *Nature Reviews Cardiology*, vol. 7, no. 9, pp. 528–536, Sep. 2010, doi: 10.1038/nrcardio.2010.115.

[47] G. Pugliese, C. Iacobini, C. B. Fantauzzi, and S. Menini, "The dark and bright side of atherosclerotic calcification," *Atherosclerosis*, vol. 238, no. 2, pp. 220–230, Feb. 2015, doi: 10.1016/j.atherosclerosis.2014.12.011.

[48] C. L. Lendon, M. J. Davies, G. V. R. Born, and P. D. Richardson, "Atherosclerotic plaque caps are locally weakened when macrophages density is increased," *Atherosclerosis*, vol. 87, no. 1, pp. 87–90, Mar. 1991, doi: 10.1016/0021-9150(91)90235-U.

[49] Z. Teng *et al.*, "A uni-extension study on the ultimate material strength and extreme extensibility of atherosclerotic tissue in human carotid plaques," *Journal of Biomechanics*, vol. 48, no. 14, pp. 3859–3867, Nov. 2015, doi: 10.1016/j.jbiomech.2015.09.037.

[50] J. Rieber *et al.*, "Diagnostic accuracy of optical coherence tomography and intravascular ultrasound for the detection and characterization of atherosclerotic plaque composition in ex-vivo coronary specimens: a comparison with histology," *Coronary Artery Disease*, vol. 17, no. 5, pp. 425–430, Aug. 2006.

[51] P. J. Bendick, J. L. Glover, R. Hankin, M. K. Reilly, M. C. Dalsing, and B. F. Waller, "Carotid Plaque Morphology: Correlation of Duplex Sonography with Histology," *Annals of Vascular Surgery*, vol. 2, no. 1, pp. 6–12, Jan. 1988, doi: 10.1016/S0890-5096(06)60771-1.

[52] F. Otsuka, K. Sakakura, K. Yahagi, M. Joner, and R. Virmani, "Has Our Understanding of Calcification in Human Coronary Atherosclerosis Progressed?," *Arteriosclerosis, Thrombosis, and Vascular Biology*, vol. 34, no. 4, pp. 724–736, Apr. 2014, doi: 10.1161/ATVBAHA.113.302642.

[53] A. Meershoek *et al.*, "Histological evaluation disqualifies IMT and calcification scores as surrogates for grading coronary and aortic atherosclerosis," *International Journal of Cardiology*, vol. 224, pp. 328–334, Dec. 2016, doi: 10.1016/j.ijcard.2016.09.043.

[54] R. M. Cahalane, H. E. Barrett, J. M. O'Brien, E. G. Kavanagh, M. A. Moloney, and M. T. Walsh, "Relating the mechanical properties of atherosclerotic calcification to radiographic density: A nanoindentation approach," *Acta Biomaterialia*, vol. 80, pp. 228–236, Oct. 2018, doi: 10.1016/j.actbio.2018.09.010.

[55] H. E. Barrett, E. M. Cunnane, E. G. Kavanagh, and M. T. Walsh, "On the effect of calcification volume and configuration on the mechanical behaviour of carotid plaque tissue," *Journal of the Mechanical Behavior of Biomedical Materials*, vol. 56, pp. 45–56, Mar. 2016, doi: 10.1016/j.jmbbm.2015.11.001.